

# Simulations of the formation of stellar discs in the Galactic centre via cloud-cloud collisions

Alexander Hobbs\* and Sergei Nayakshin

*Dept. of Physics & Astronomy, University of Leicester, Leicester, LE1 7RH, UK*

8 March 2019

## ABSTRACT

Young massive stars in the central parsec of our Galaxy are best explained by star formation within at least one, and possibly two, massive self-gravitating gaseous discs. With help of numerical simulations, we here consider whether the observed population of young stars could have originated from a large angle collision of two massive gaseous clouds at  $R \simeq 1$  pc from Sgr A\*. In all the simulations performed, the post-collision gas flow forms an inner, nearly circular gaseous disc and one or two eccentric outer filaments, consistent with the observations. Furthermore, the radial stellar mass distribution is always very steep,  $\Sigma_* \propto R^{-2}$ , again consistent with the observations. All of our simulations produce discs that are warped by between  $30^\circ$  to  $60^\circ$ , in accordance with the most recent observations. The 3D velocity structure of the stellar distribution is sensitive to initial conditions (e.g., the impact parameter of the clouds) and gas cooling details. For example, the runs in which the inner disc is fed intermittently with material possessing fluctuating angular momentum result in multiple stellar discs with different orbital orientations, contradicting the observed data. In all the cases the amount of gas accreted by our inner boundary condition is large, enough to allow Sgr A\* to radiate near its Eddington limit over  $\sim 10^5$  years. This suggests that a refined model would have physically larger clouds (or a cloud and a disc such as the circumnuclear disc) colliding at a distance of a few parsecs rather than 1 parsec as in our simulations.

**Key words:** accretion, accretion discs – Galaxy: centre – stars: formation – galaxies: active

## 1 INTRODUCTION

The power output of the central parsec of our Galaxy is dominated by young (aged  $6 \pm 1$  million years) massive “He-I” stars (Krabbe et al., 1995). Many of these stars are located in a well-defined thin disc structure that rotates clockwise as seen on the sky (Levin & Beloborodov, 2003; Genzel et al., 2003; Paumard et al., 2006). The remaining stars can be classified as a second more diffuse disc rotating counter clockwise (Genzel et al., 2003; Paumard et al., 2006) although the statistical significance of this feature is disputed (Lu et al., 2006). Stars appear to be on more eccentric orbits in the second disc (Paumard et al., 2006; Lu et al., 2006). The bright He-I stars seem to be excluded from the central arcsecond ( $1'' \approx 0.04$  pc when viewed from the  $\approx 8$  kpc distance to the Galactic Centre (GC)), which instead contains at least a dozen less massive but still quite young B-type stars (Ghez et al., 2003; Ghez et al., 2005). These

stars (commonly referred to as S-stars in the Galactic Centre community) appear to be on rather eccentric orbits distributed without any notable preference to a planar configuration (e.g., Eisenhauer et al., 2005; Lu et al., 2006). At present it is not clear if the S-stars are physically related to the more massive “disc”-stars, as the initial orbits of the S-stars could have been very different from their present day ones due to resonant relaxation processes (Hopman & Alexander, 2006). Thus, in this paper we shall concentrate on the puzzle of the young massive stars found outside the inner arcsecond as these present us with a cleaner laboratory environment.

Gerhard (2001) suggested that the stars may have been formed at a distance of tens of parsecs in a massive star cluster. The cluster’s orbit would then decay through dynamical friction with the background stars, and eventually the stars would form a disc populated by stars on eccentric orbits (e.g., Hansen & Milosavljević, 2003; Kim et al., 2004; Gürkan & Rasio, 2005; Levin et al., 2006). However, infrared observations find no young massive stars outside the central  $\sim 0.5$  pc (Paumard et al., 2006) which

\* E-mail: alexander.hobbs@astro.le.ac.uk

should be present in this model. In addition, Chandra X-ray limits (Nayakshin & Sunyaev, 2005) constrain the number of X-ray emitting Young Stellar Objects to well below what is expected in the cluster disruption scenario.

An alternative model is the in-situ model in which stars form inside a self-gravitating gaseous disc (e.g., Levin & Beloborodov, 2003; Nayakshin & Cuadra, 2005; Paumard et al., 2006). In fact, theorists had expected gaseous massive discs around supermassive black holes to form stars or planets (e.g., Paczyński, 1978; Kolykhalov & Sunyaev, 1980; Shlosman & Begelman, 1989; Golin & Zilman, 1996; Camm et al., 2001; Goggin et al., 2003). long before the properties of the young stars in the GC became known. Recently, Nayakshin et al. (2007) have numerically simulated the fragmentation process of a geometrically thin gaseous disc of mass  $\gtrsim 10^4 M_\odot$  for conditions appropriate for our GC (albeit with a rather simple cooling prescription) and found a top-heavy mass function for the stars formed there. Alexander et al. (2008) extended numerical studies to the fragmentation of eccentric accretion disks.

However, the in-situ model has not so far addressed in detail the origin of the gaseous discs themselves, although similar discs are believed to exist in AGN and quasars. Indeed, sub-parsec massive gaseous discs are invoked as means of feeding supermassive black holes' immense appetite for gaseous fuel (e.g. Frank et al., 2002). Such discs are actually observed as the sites of maser emission in some of the nearby galactic centres (Miyoshi et al., 1995). But Sgr A\* is currently not a member of the AGN club, let alone the even more powerful and elitist quasar community. Indeed, Sgr A\* bolometric luminosity is around  $\sim 10^{-9}$  of its Eddington limit (e.g., Narayan, 2002; Baganoff et al., 2003). The amount of ionised gas currently present in the inner parsec is estimated at perhaps a mere hundred solar masses (Paumard et al., 2004). There are also tight observational constraints (Falcke & Melia, 1997; Cuadra et al., 2003) on the presence of an optically thin disc on smaller scales (say 0.01 pc or less).

We believe that the requisite gaseous discs could not have been assembled by viscous transport of angular momentum as is expected to be the case in other systems (Shakura & Sunyaev, 1973; Frank et al., 2002). The viscous time scale of a thin, marginally self-gravitating disc can be estimated as  $t_{\text{visc}} = (M_{\text{bh}}/M_{\text{disc}})^2 (\alpha\Omega)^{-1}$ , where  $M_{\text{bh}} \approx 3.5 \times 10^6 M_\odot$  and  $M_{\text{disc}}$  are masses of the blackhole and the disc, respectively, and  $\Omega$  is the Keplerian angular frequency. For  $\alpha = 0.1$  and  $M_{\text{disc}} \approx 10^4 M_\odot$  (reasons for this choice of mass are discussed in Nayakshin et al. (2006)),  $t_{\text{visc}} \sim 3 \times 10^7$  years at  $R = 0.03$  parsec, the inner edge of the discs (Paumard et al., 2006), and  $10^9$  years at 0.3 parsec. These times are very long compared with the age of the stellar systems. In fact, the gaseous discs would have to evolve even faster as the two stellar systems are co-eval within one million years (Paumard et al., 2006).

It is also not clear that one should expect any sort of a viscous quasi-steady state for the gas in our Galactic Centre. There is no strong evidence for other similar star formation events in the central parsec within the last  $\sim 10^8$  years. Therefore, the one-off star formation event appears to be best explained by a one-off deposition of gas within the central parsec. There are several ways in which this could have happened, e.g. a Giant Molecular Cloud (GMC) with a sub-parsec impact parameter (in relation to Sgr A\*) could have

self-collided and become partially bound to the central parsec (e.g., Nayakshin & Cuadra, 2005). Alternatively, a GMC could have struck the Circumnuclear Disc (CND) located a few parsecs away from Sgr A\*, and then created gas streams that settled into the central parsec.

It is very hard to estimate the probability of a cloud-cloud collision in the central part of the Galaxy. Hasegawa et al. (1994) estimated the rate of GMC collisions as one per 20 Myrs in the central 100 pc, but the estimate is very uncertain due to the lack of knowledge about the size distribution of GMCs. However, there is observational evidence that GMCs can be put on orbits significantly different from the simple circular orbits seen in the inner Galaxy. Stolte et al. (2008) recently measured the proper motions of the Arches star cluster. This star cluster is about 2.5 million years old and has a mass in excess of  $10^4 M_\odot$  (e.g., Figer, 2004). It is presently about 30 pc away from Sgr A\* in projection. Its orbit must be strongly non-circular as its 3D velocity is over 200 km/sec in the region where the circular velocity is only  $\sim 110$  km/sec. Therefore, this suggests that massive GMCs can be on highly non-circular orbits. It does not seem implausible that one of these clouds would pass within a few parsec of Sgr A\*.

In this paper we explore such a one-off collision event in a very simple setup (§3). We allow two massive, uniform and spherical clouds on significantly different orbits to collide with each other one parsec away from Sgr A\*. The resulting gas dynamics, in particular the way in which gas settles into the inner parsec, is the focus of our effort here. We find that the collision forms streams of gas with varying angular momentum, both in magnitude and direction. Parts of these streams collide and coalesce to form a disc, and remaining parts form one or more orbiting filaments. As the gas cools, it becomes self-gravitating and stars are born, usually in both the disc and the filaments. This overall picture is discussed in §4.1. A reader mainly interested in a comparison between the simulations and observations may find sections 5, 6 and 7 most relevant<sup>1</sup>. In §7.2 we argue that our simulation results suggest that the location of the original impact was somewhat further away from Sgr A\* than we assumed here, e.g., perhaps a few parsecs.

## 2 NUMERICAL METHODS

The numerical approach and the code used in this paper is the same as in Nayakshin et al. (2007) with only slight modifications. We employ GADGET-2, a smoothed particle hydrodynamic (SPH)/N-body code (Springel, 2005). The Newtonian N-body gravitational interactions of particles in the code are calculated via a tree algorithm. Artificial viscosity is used to resolve shocks in the gas. Gas cools according to  $du/dt = -u/t_{\text{cool}}(R)$ , where cooling time depends on radius as

$$t_{\text{cool}}(R) = \beta t_{\text{dyn}}(R) \quad (1)$$

<sup>1</sup> For movies of the simulations the reader is directed to <http://www.astro.le.ac.uk/~aph11/movies.html>

where  $t_{\text{dyn}} = 1/\Omega$  and  $\Omega = (GM_{\text{bh}}/R^3)^{1/2}$  is the Keplerian angular velocity, and  $\beta$  is a dimensionless parameter. This approach is motivated by simulations of marginally stable self-gravitating gaseous discs, where  $\beta$  is expected to be of the order of a few (Gammie, 2001; Rice et al., 2005). In the problem at hand,  $\beta$  would most likely be much smaller than this during the collision phase of the clouds as gas can heat up to high temperatures (see §7.2), but it could be much larger than unity when gas cools into a geometrically thin disc or a thin filament. In the framework of our simplified approach, and given numerical limitations, we only consider two values for  $\beta$ . The  $\beta = 1$  tests approximate the situation when cooling is inefficient, whereas  $\beta = 0.3$  cases correspond to rapid cooling. Each of our runs used between 3 to 6 months of integration time on 12 processors in parallel.

Gas moves in the gravitational potential of Sgr A\*, modelled as a motionless point mass with  $M_{\text{bh}} = 3.5 \times 10^6 M_{\odot}$  (Reid et al., 1999) at the origin of the coordinate system, and a much older relaxed isotropic stellar cusp. For the latter component we use the stellar density profile derived from near-IR adaptive optics imaging by Genzel et al. (2003):

$$\frac{\rho_*(R)}{\rho_{*0}} = \begin{cases} \left(\frac{R}{R_{\text{cusp}}}\right)^{-1.4}, & R < R_{\text{cusp}} \\ \left(\frac{R}{R_{\text{cusp}}}\right)^{-2}, & R \geq R_{\text{cusp}} \end{cases} \quad (2)$$

where  $R_{\text{cusp}} = 10$  arcseconds ( $\approx 0.4$  pc), and  $\rho_{*0} = 1.2 \times 10^6 M_{\odot}/\text{pc}^3$ .

Note that the enclosed stellar cusp mass is approximately  $6 \times 10^5 M_{\odot}$  at  $R = R_{\text{cusp}}$  and equals Sgr A\* mass at  $R \sim 1.6$  pc. We do not include the gravitational potential of the putative stellar mass black hole cluster around Sgr A\* (e.g., Morris, 1993; Miralda-Escudé & Gould, 2000), as at present its existence and exact properties are highly uncertain (Freitag et al., 2006; Schödel et al., 2007; Deegan & Nayakshin, 2007).

Star formation and accretion in SPH is traditionally modelled via the “sink particle” formalism (Bate et al., 1995), where gravitationally contracted gas haloes are replaced by the collisionless sink particles of same mass. We follow the same recipe, allowing Sgr A\* to accrete all gas particles that are within  $R_{\text{acc}} \sim 0.1$  arcsecond (exact values vary between different cooling parameters, cf. §3). This is significantly smaller than the inner radius of the observed “disc” population of young massive stars, i.e.,  $\sim 1''$  (Paumard et al., 2006).

To model star formation, new sink particles are introduced when gas density exceeds

$$\rho_{\text{crit}} = \rho_0 + A_{\text{col}}\rho_{\text{BH}} \quad (3)$$

where  $\rho_0 = 5 \times 10^{-11} \text{ g cm}^{-3}$ ,  $\rho_{\text{BH}}$  is the tidal density, and  $A_{\text{col}} = 60$  (these values are based on tests performed in Nayakshin et al. (2007), which found that the results are not sensitive to the exact values of  $\rho_0$  and  $A_{\text{col}}$ , provided they are sufficiently large). For reasons fully explained in Nayakshin et al. (2007), we distinguish between “first cores” – star particles with  $M \leq M_{\text{core}} = 0.1 M_{\odot}$ , and “stars” with  $M > M_{\text{core}}$ . Physically, first cores represent massive gaseous clumps that have not yet collapsed to stellar densities, and thus have finite sizes that are set to  $R_{\text{core}} = 10^{14}$  cm. First cores are allowed to merge with each other if they pass within a distance  $d < 2R_{\text{core}}$ .

In contrast, stars are not allowed to merge, but can accrete first cores if they pass within a distance of  $R_{\text{core}}$ . Accretion of gas onto stars and proto-stars is calculated using the Bondi-Hoyle formalism, with the accretion rate given by

$$\dot{M} = 4\pi\rho \frac{(GM)^2}{(\Delta v^2 + c_s^2)^{3/2}} \quad (4)$$

where  $M$  is the mass of the sink particle,  $\rho$  is the ambient gas density,  $c_s$  is the sound speed, and  $\Delta v$  is the relative velocity between the gas and the accreting particle. The accretion rate is capped at the Eddington accretion rate:

$$\dot{M}_{\text{Edd}} = \frac{4\pi m_p R_* c}{\sigma_T} \quad (5)$$

where  $m_p$  is the proton mass,  $c$  the speed of light and  $\sigma_T$  the Thomson scattering cross-section. Note that this expression depends only on the size of the object,  $R_*$ . For first cores,  $R_* = R_{\text{core}}$ , which yields a very high accretion rate limit of almost a solar mass per year for  $R_{\text{core}} = 10^{14}$  cm. For stars, we use the observational results of Demircan & Kahraman (1991; Gorda & Svechnikov (1998):

$$\frac{R}{R_{\odot}} = 1.09 \left(\frac{M}{M_{\odot}}\right)^{0.969} \quad \text{for } M < 1.52 M_{\odot}, \quad (6)$$

$$\frac{R}{R_{\odot}} = 1.29 \left(\frac{M}{M_{\odot}}\right)^{0.6035} \quad \text{for } M > 1.52 M_{\odot}. \quad (7)$$

For  $R = R_{\odot}$ , this yields an Eddington accretion rate limit of  $\sim 5 \times 10^{-4} M_{\odot} \text{ year}^{-1}$ . The actual gas particles that are then accreted by the sink particle are chosen from its neighbours via the stochastic SPH method of Springel (2005). The mass and momentum of the SPH particles accreted are added to that of the respective sink particle.

Finally, we shall acknowledge that this plausible star formation *prescription* cannot possibly do justice to the full complexity of the physical star formation process. Therefore, the stellar mass function obtained in our simulations should not be trusted in detail. However, our focus is on the dynamics of gas as it settles into a disc or a filamentary structure. When star formation does occur, the gas temperature is very much smaller than the virial temperature in the simulated region ( $\gtrsim 10^6 K$ ). Gas orbits thus determine the resulting stellar orbits which we compare to the observed ones. We believe that this important aspect of our simulations is reliably modelled.

The set of units used in the simulations is  $M_u = 3.5 \times 10^6 M_{\odot}$ , the mass of Sgr A\* (e.g., Schödel et al., 2002),  $R_u = 1.2 \times 10^{17} \text{ cm} \approx 0.04 \text{ pc}$ , equal to 1” when viewed from the  $\approx 8$  kpc distance to the GC, and  $t_u = 1/\Omega(R_u)$ , the dynamical time evaluated at  $R_u$ , approximately 60 years. We use  $R$  to signify distance in physical units and the dimensionless  $r = R/R_u$  throughout the paper interchangeably.

### 3 INITIAL CONDITIONS

Simulations were performed for several sets of initial conditions, all of which comprise a collision between two gas clouds at the edge of the inner parsec of the GC. The specific parameters for each run, labeled S1 to S6, can be found in Table 1. Each cloud is spherically symmetric and of uniform density, containing less than 1% of the mass of Sgr A\*. The clouds are composed of molecular hydrogen, with the

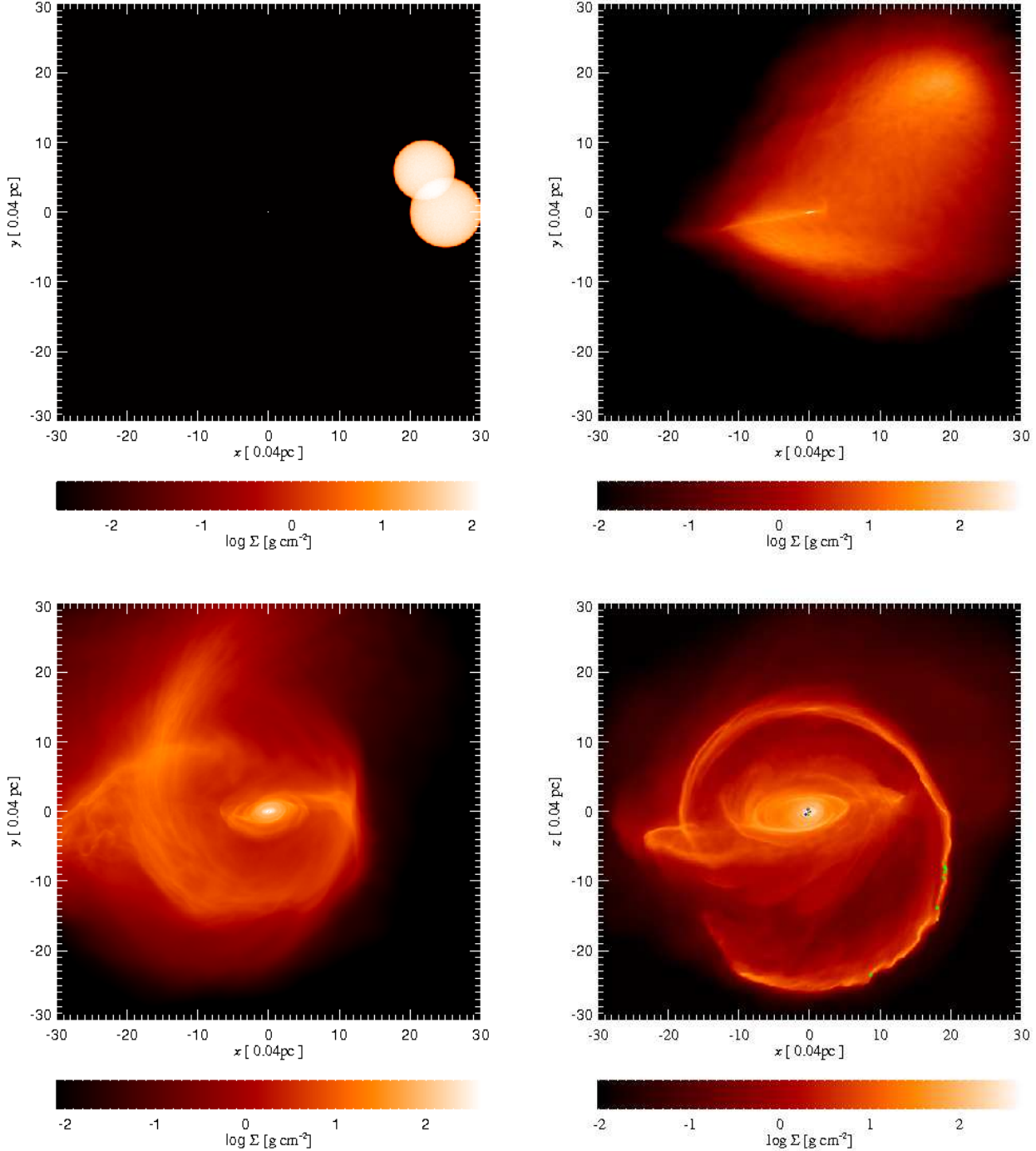


**Figure 1.** Gas surface density and star locations (in the bottom right panel) for snapshots from simulation S1 taken at times  $t = 0, 100, 250$ , and  $1000$ , left to right and top to bottom, respectively. Sgr A\* is located at  $(0,0)$ , and the line of sight is along the  $z$ -direction.

mean molecular weight set to  $\mu = 2.46$ . The initial temperature of the clouds is set to  $20\text{K}$ . A more complex model could have included a turbulent velocity and density field, but for practical purposes we limit ourselves to a smaller set of input parameters for this first study.

We define the primary to be the larger cloud, with a radius of  $R_1 = 0.2\text{ pc}$  and  $M_1 = 3.4 \times 10^4 M_\odot$ , whilst the secondary has a radius of  $R_2 = 0.172\text{ pc}$  with  $M_2 =$

$2.6 \times 10^4 M_\odot$ . The initial positions of the cloud centres are the same for all the simulations, and are given in Table 1 in dimensionless units. The initial density of the clouds is slightly above the tidal shear density at their initial locations, so the clouds are marginally stable to tidal shear by Sgr A\*.

In all the tests the initial velocity of the primary cloud is kept fixed, and is of the order of the Keplerian circular veloc-

ity for that radius. Orbits in a cusped potential are however not Keplerian. The initial specific energy and angular momentum  $l$  of a particle can be used to find the pericenter,  $r_{\text{pe}}$ , and the apocenter,  $r_{\text{ap}}$ , of the orbit. The orbit's eccentricity  $e$  is then defined via

$$\frac{1+e}{1-e} = \frac{r_{\text{ap}}}{r_{\text{pe}}} . \quad (8)$$

In our simulations particles occasionally obtain hyperbolic orbits. For analysis (plotting) purposes only, the eccentricities are capped at 1. In the stellar potential used here (equation 2), the orbit of the primary cloud is slightly eccentric, with pericentre and apocentre of 25 and 31.5 respectively, and with eccentricity  $e = 0.12$ .

The initial trajectory of the secondary cloud is varied between the tests to cover a small range of possibilities. The parameters for this trajectory in terms of pericentre, apocentre and eccentricity are given in Table 1. The collision itself is highly supersonic, as is expected for molecular gas falling into the potential well of a supermassive blackhole.

We ran tests with cooling parameter  $\beta = 1$  and  $\beta = 0.3$  (see equation 1). These values are low enough so that fragmentation would occur if and when regions of the gas became self-gravitating (Gammie, 2001; Rice et al., 2005). Since the faster cooling runs were expected to require on average shorter timesteps the accretion radius for  $\beta = 0.3$  was set to  $r_{\text{acc}} = 0.33$  whilst for  $\beta = 1$  a smaller value of  $r_{\text{acc}} = 0.06$  was used.

## 4 SIMULATIONS

### 4.1 Overall picture

In all of our simulations, the clouds undergo an off-centre collision at time  $t \sim 10$  in code units ( $\approx 600$  years). As the cooling time is longer than the collision time,  $t_{\text{coll}} \sim (R_1 + R_2)/(|\mathbf{v}_1 - \mathbf{v}_2|)$ , the clouds heat up significantly and hence initially expand considerably. This thermal expansion also modifies the velocity of the different parts of the clouds by giving the gas velocity “kicks”. The net result is a distribution of gas velocities that is much broader than what one would get if the two clouds simply stuck together, i.e. in an inelastic collision.

The collision and resultant mixing of the clouds leads to angular momentum cancellation in some parts of the gas. Regions of gas that acquire smaller angular momenta infall to the respective circularisation radius on the local dynamical time. A small scale disc around the black hole is thus formed on this timescale. Regions of the clouds that did not directly participate in the collision are affected less and retain more of their initial angular momentum. These regions are initially not self-gravitating, and so are sheared by the tidal field of Sgr A\*. They later cool and result in filaments of length comparable to the initial sizes of the clouds' orbits.

As time progresses, parts of the filaments collide with each other or with the inner disc if the pericentres of their orbits are small enough. The inner disc therefore gains mass in an asymmetric non-planar manner, leading to the disc becoming warped and changing its orientation with time.

Eventually, due to gravitational collapse, high density gas clumps are formed. Sink particles are introduced inside

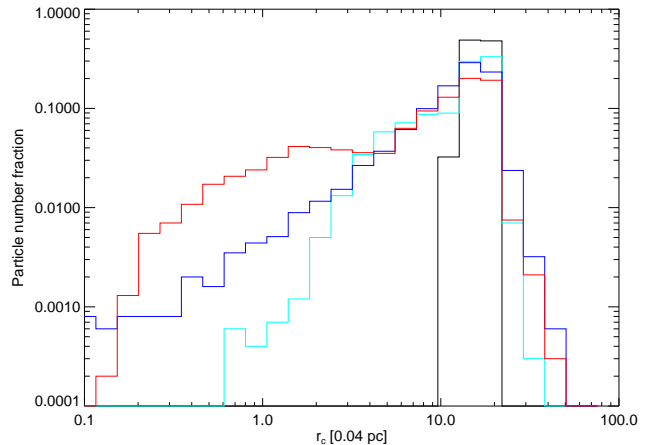


**Figure 2.** The distribution of SPH particles over the circularisation radius of their orbits. The black, magenta, blue and red curves correspond to times  $t = 0, 25, 50, 500$ , respectively. As the result of angular momentum cancellation due to shocks, particles “leak” to small radii, establishing there a disc that eventually forms stars.

these clumps and are allowed to grow in mass via gas accretion and mergers with first cores as explained in §2. Star formation takes place in all of our simulations. Although the precise locations and the stellar mass distributions differ we always end up with stellar populations forming in two distinct locations – in the disc around the black hole and in the outer filament(s). Disc populations generally have top-heavy mass functions whilst filament populations always consist entirely of low-mass stars; however, as noted in §2, the mass spectrum of stars formed depends on a very simple prescription (e.g., see Nayakshin et al., 2007). We expect the mass spectrum of our models to change when more realistic cooling and feedback physics is included.

### 4.2 SIMULATION S1

#### 4.2.1 Gas dynamics

Figure 1 presents four snapshots of simulation S1 showing gas column density and positions of the stars viewed along the  $z$ -axis.

The initial mass deposition into the central few arcseconds forms a small-scale disc that changes its orientation by about  $30^\circ$  with time, stabilising by  $t \sim 300$ . As a result of the small impact parameter of the cloud collision, the secondary cloud is largely destroyed and does not collapse into a coherent filament. Instead, the diffuse gas left over from the impact gradually accretes onto the disc that forms around the black hole, growing it in mass and radius. The inner disc therefore ends up extending out to  $r \sim 10$  in code units. The gas left over from the primary cloud collapses into a filament which orbits at a larger radius, separate from the disc.

It is useful to analyse the re-distribution of the gas as a result of the collision in terms of orbital parameters, namely, angular momentum and eccentricity. Gas with specific angular momentum  $l = |\mathbf{r} \times \mathbf{v}|$  circularises at the circularisation

**Table 1.** Initial conditions of the simulations presented in the paper. The meaning of the symbols in the Table are:  $\beta$  is the cooling parameter,  $\mathbf{r}_1$ ,  $\mathbf{r}_2$ ,  $\mathbf{v}_1$ ,  $\mathbf{v}_2$  are the initial positions and velocity vectors of the two clouds, respectively;  $r_{\text{pe}}$  and  $r_{\text{ap}}$  are the pericentres and the apocentres of the two clouds;  $e$  is their orbit’s eccentricity;  $\theta$  is the angle between the orbital planes of the clouds, and  $b$  is the impact parameter.

ID	$\beta$	$\mathbf{r}_1$	$\mathbf{r}_2$	$\mathbf{v}_1$	$\mathbf{v}_2$	$ \mathbf{v}_1 - \mathbf{v}_2 $	$r_{1,\text{pe}}$	$r_{1,\text{ap}}$	$r_{2,\text{pe}}$	$r_{2,\text{ap}}$	$e_1$	$e_2$	$\theta$ ( $^\circ$ )	$b$
S1	1	(25,0,0)	(22,6,7)	(0,0.2,0)	(0,-0.11,-0.21)	0.37	25	31.5	12.8	29.5	0.12	0.39	116	3.8
S2	1	(25,0,0)	(22,6,7)	(0,0.2,0)	(0,-0.21,-0.11)	0.42	25	31.5	13.2	29.1	0.12	0.38	151	6.8
S3	0.3	(25,0,0)	(22,6,7)	(0,0.2,0)	(0,-0.11,-0.21)	0.37	25	31.5	12.8	29.5	0.12	0.39	116	3.8
S4	0.3	(25,0,0)	(22,6,7)	(0,0.2,0)	(0,-0.21,-0.11)	0.42	25	31.5	13.2	29.1	0.12	0.38	151	6.8
S5	1	(25,0,0)	(22,6,7)	(0,0.2,0)	(0.16,-0.11,-0.21)	0.41	25	31.5	21.8	43.1	0.12	0.33	120	2.4
S6	1	(25,0,0)	(22,6,7)	(0,0.2,0)	(0.16,-0.21,-0.11)	0.45	25	31.5	21.5	43.4	0.12	0.34	147	5.3

radius,  $r_c$ , given by the relation

$$l^2 = GM(r_c)r_c, \quad (9)$$

where  $M(r)$  is the total enclosed mass within radius  $r$ . Figure 2 shows the distribution of gas particles as a function of the circularisation radius of their orbits as a histogram for several snapshots. At time  $t = 0$ , the distribution is highly peaked around the clouds’ initial circularisation radii. Due to the collision, however, a tail to small  $r_c$  appears in the distribution very quickly. This is not due to viscous angular momentum transport, as in thin accretion discs, but is rather due to cancellation of oppositely directed angular momentum components in shocks. Some of the gas particles acquire particularly small angular momenta and hence fall to small radial separations from Sgr A\* on nearly radial trajectories. Particles with  $r_c < r_{\text{acc}}$  are in general accreted by Sgr A\* in our formalism (unless their orbit is changed by interactions before they make it inside  $r_{\text{acc}}$ ). Particles with  $r_c > r_{\text{acc}}$  settle into a thin rotationally supported disc, or into sheared out filaments (the remains of the clouds). Note that due to the complicated geometry, some gas particles pass through shocks several times before reaching their final destination (i.e. the disc).

Figure 3 shows the profiles of orbital eccentricity (defined on radial shells) plotted for several snapshots. These profiles again show that soon after the collision the inner part of the computational domain is dominated by gas on plunging – high eccentricity – orbits. At later times finite net angular momentum of gas and shocks force the gas to circularise outside the inner boundary of the simulation domain. It is notable that gas circularises faster at smaller radii, which is naturally expected as the orbital time is shortest there. Therefore, towards later times, nearly circular gaseous orbits are established in the innermost few arcseconds, whereas eccentric ones dominate at larger radii.

#### 4.2.2 Structures in angular momentum space

The various structures that are formed in the simulation can also be identified by the orientation of the angular momentum vector  $\mathbf{L}$  of a particle’s orbit. We define two angles,  $\theta$  and  $\phi$ , so that  $L_z = |\mathbf{L}| \cos \theta$ , where  $L_z$  is the  $z$ -component of  $\mathbf{L}$ , and  $\tan \phi = L_y/L_x$ . We then plot the values of these an-

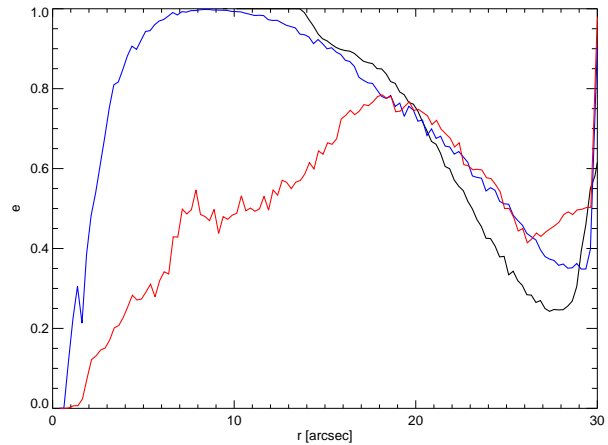


**Figure 3.** Gas eccentricity defined on radial shells as a function of the shell’s radius at different times. Black, blue and red curves corresponding to time  $t = 50, 100$  and  $250$ . Note that initially only gas on near-plunging high eccentricity orbits arrives in the innermost region, but with time gas circularises to  $e \ll 1$ .

gles for individual SPH particles and stars in the Aitoff projection. As the number of SPH particles is too large to show each particle, we show only a small fraction of these, randomly chosen from the total number. This procedure keeps the resulting maps reasonably clear while also preserving the shape of the distribution.

The result is shown in Figure 4 for a selection of times. At  $t = 0$  all the gas particles are concentrated in the two clouds, with the finite spread in the distribution arising as a result of all the particles within a cloud having the same velocity whilst possessing a finite spread in positions about the centre. The difference in the orientations of the two clouds is almost  $120^\circ$  (cf. Table 1). By  $t = 100$ , the clouds have collided and the gas particles have experienced ‘kicks’ in different directions, filling the entire range in  $\theta$ . The  $\phi$  values are restricted to a rather narrow band running about  $\phi = +90^\circ$  and  $\phi = -90^\circ$  lines. Note that this band structure forms a plane  $L_x \approx 0$  in  $\mathbf{L}$ -space. This is expected since gas particles experience the collision close to the  $x$ -axis, i.e.,



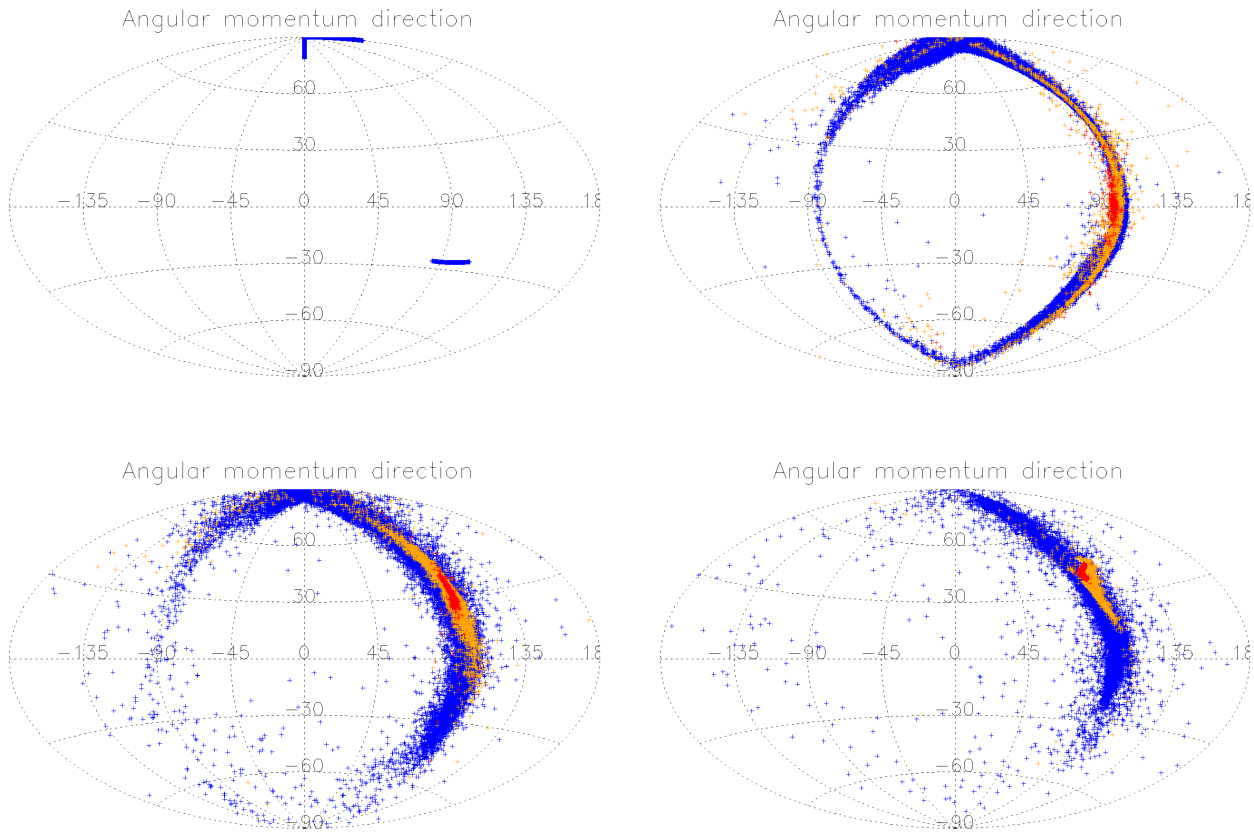


**Figure 4.** Angular momentum direction in terms of the azimuthal,  $\theta$ , and the polar,  $\phi$ , angles. The frames are shown at  $t = 0, 100, 250, 1000$ . Gas particles are colour-coded;  $r \leq 1''$  (red),  $r \leq 5''$  (orange),  $r > 5''$  (blue).

where  $y/x \approx z/x \approx 0$ . Therefore, the  $x$ -component of the resulting angular momentum,  $L_x = yv_z - zv_y$  is very small.

The plots are colour-coded to show the behaviour of the gas in the inner arcsecond (red), the inner 5 arcseconds (orange), and outside the inner 5 arcseconds (blue). Whilst the distribution just after the collision is fairly spread out for all the three regions, we note a clear difference at later times. In particular, the innermost disc occupies a region positioned in between the two clouds’ original positions. It is also the least spread out structure, defining a thin disc which is only slightly warped by  $t = 1000$ . The innermost disc orientation does evolve with time, however, as we noted already in §4.1, since matter infall on the disc continues throughout the simulation.

The gas coloured in orange demonstrates a greater extent of warping, and the region outside this ( $> 5''$ ) cannot even be classified into a single structure (cf. Figure 1). Nevertheless, it is clear that the inner and outer gas distributions are similarly oriented with respect to each other, with the majority of the outer gas angular momentum distributed in  $\theta$  and  $\phi$  between the initial values of the clouds.

#### 4.2.3 Star formation

Stars in S1 form in both the disc and the primary filament. In the disc, stars form first in the inner arcsecond at  $t \sim$

900 and later at a radius of  $\sim 5 - 8''$  at  $t \sim 1700$ . In the filament, star formation is approximately co-eval with the inner arcsecond population and occurs at a radius of  $\sim 15 - 25''$ . Mass functions in the disc become top-heavy relatively quickly (as the dynamical time is short), with high-mass stars ( $M \sim 100 M_\odot$ ) appearing by  $t \approx 1100$ , whilst stars in the filament remain entirely low-mass ( $\sim 0.1 - 1 M_\odot$ ) for the duration of the simulation. The disc and filament stellar orbits are inclined to each other by  $\sim 60^\circ$ , similar to the gas orbital inclination.

All three stellar populations can be seen in Figure 5; the “inner disc” population (within the inner  $1 - 2''$ ), the “mid-range disc” population ( $5 - 8''$ ) and the “filament” population. The orbits in the inner disc population are almost circular,  $e \sim 0.05$ , whilst stars in the mid-range disc have eccentricities of  $e \sim 0.2$ . Both of these are therefore in good agreement with the clockwise feature of the observations Lu et al. (2006). The orbit of the filament population is also eccentric, with  $e \gtrsim 0.2$ . This is in reasonable agreement with the corresponding counter-clockwise feature of the observations, although the eccentricity of the latter is considered to be somewhat higher with  $e \sim 0.8$  (Paumard et al., 2006).

### 4.3 SIMULATION S2

#### 4.3.1 Gas dynamics

The simulation S2 is set up identically to S1 except for the initial velocity of the secondary cloud (cf. Table 1). As the result, the angle between the orbital plane of the two clouds is greater,  $\theta \sim 150^\circ$ , and the collision between the clouds is more grazing (i.e. the impact parameter  $b$  is greater).

Smaller fractions of the clouds' mass are therefore involved in a bodily collision, and as a result the two clouds survive the initial collision better. Indeed, comparing the S1 and S2 simulations in Figure 5, one sees that in the latter simulation most of the secondary cloud actually does survive the collision. This cloud forms a clockwise filament which was largely absent in simulation S1. Both S2 filaments contain a greater amount of mass than their S1 counterpart.

On the other hand, the parts of the clouds involved in the direct collision experience a stronger shock in S2 than they do in S1 as the velocity vectors in the former are almost directly opposing. Thus, despite the larger impact parameter, the stronger angular momentum cancellation in S2 creates an inner  $r < 1$  disc as massive as that in S1. However, the “mid-range” disc largely fails to form in S2.

Another difference between S1 and S2 is the evolution and the structure of the inner gaseous disc. In both simulations the angular momentum of the gas infalling onto the discs evolves with time, and hence the mid-planes of both discs undergo a change of orientation in both  $\theta$  and  $\phi$  (we refer to this as ‘midplane rotation’). However the infalling gas seems to be more intermittent in S2 compared to S1, possessing a larger range of angular momentum. Whilst in S1 the accreting gas largely adds to the existing disc, creating one large, relatively warped disc, in S2 the infalling gas causes enhanced disc midplane rotation, and at later times ( $t \sim 400$ ), actually creates a second disc around the first at a different orientation. Over time, the first (inner) disc aligns somewhat with the second one. This process repeats at larger radii as gas continues to fall in with a different orientation of angular momenta to that of the existing disc. The eventual result is that the S2 disc is significantly more warped than its S1 counterpart. Figure 7 compares the inner discs of S1 and S2 in the process of forming.

The difference in gas distribution between the two simulations can be also noted by looking at the respective histogram plots of circularisation radius (Figure 2 and Figure 8 respectively). A tail to small  $r_c$  appears faster in S2, by  $t = 25$  rather than  $t = 50$  in S1. The radial profile of gas in S2 by  $t = 500$  has a gap between the inner and outer distributions, and is far more peaked than the flatter, more even distribution of S1 at an equivalent time.

#### 4.3.2 Star formation

Stars form earlier in S2 than in S1, and they form in the disc first, by  $t = 400$ . The preferential sites of star formation in the disc appear to be dense concentric ring structures – see Figure 7 – we discuss these in more detail in §4.6. Owing to the significantly peaked distribution of gas (Figure 8) in S2, there is a far greater amount of star formation at both small and large radii compared to S1 at an equivalent time. This can be seen in Figure 5. The stars formed in the disc are again top-heavy and in the filaments are again low-mass.

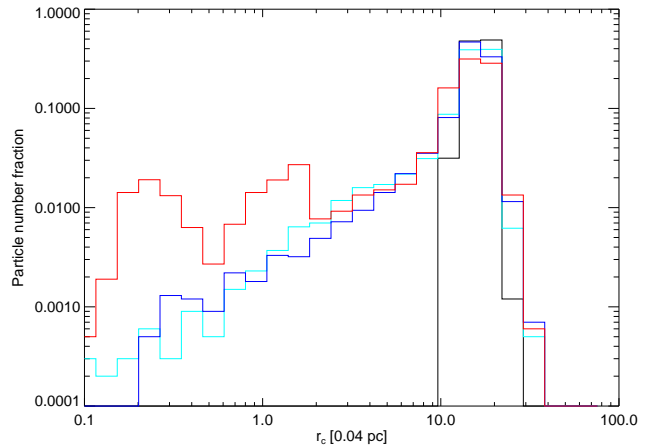


**Figure 8.** The distribution of SPH particles over circularisation radius for simulation S2. The black, magenta, blue and red curves correspond to times  $t = 0, 25, 50, 500$  respectively.

The stars in the filaments show a tendency to form inside clusters – this effect is discussed in more detail in §4.4.

#### 4.3.3 Structures in angular momentum space

Figure 6 shows the orientation of the angular momentum vectors for orbits of gas (in grey) and stars (in colour) in the Aitoff projection, for S1 and S2 at the same times as in Figure 5. We identify stars of different masses using different colours; green ( $0.1 - 1 M_\odot$ ), cyan ( $1 - 10 M_\odot$ ), blue ( $> 10 M_\odot$ ), and magenta ( $> 150 M_\odot$ ). As already noted, in S2 the secondary cloud largely survives the collision and forms a stream, which later collapses into stars. These stars can be found at the original orientation of that cloud in the right panel in Figure 6 (green at around  $\theta = -60^\circ$ ). The primary and secondary outer stellar populations are therefore inclined at a large angle of  $\theta \simeq 150^\circ$  to each other, as is expected since they are the stellar remnants of the original clouds. The angular momentum vector of the disc stellar population is oriented at an angle in between that of the two outer stellar populations.

The other interesting feature of these plots is that the stellar disc is strongly warped. The origin of this warp is in the warping of the gaseous disc rather than any secular evolution once the stars have formed.

### 4.4 SIMULATIONS S3 & S4

S3 and S4 are identical to S1 and S2 respectively, except for the value of the cooling parameter  $\beta$  which is set to a lower value of 0.3.

#### 4.4.1 Gas dynamics

To show the effect of the faster cooling, Figure 9 contrasts gas surface density plots of simulations S1 and S3 at time  $t = 150$ . The bulk dynamics of S3 are the same as in S1, but apart from the innermost few arcseconds, maximum gas densities are higher in S3 than they are in S1. This is natural as faster cooling gas can be compressed to higher densities



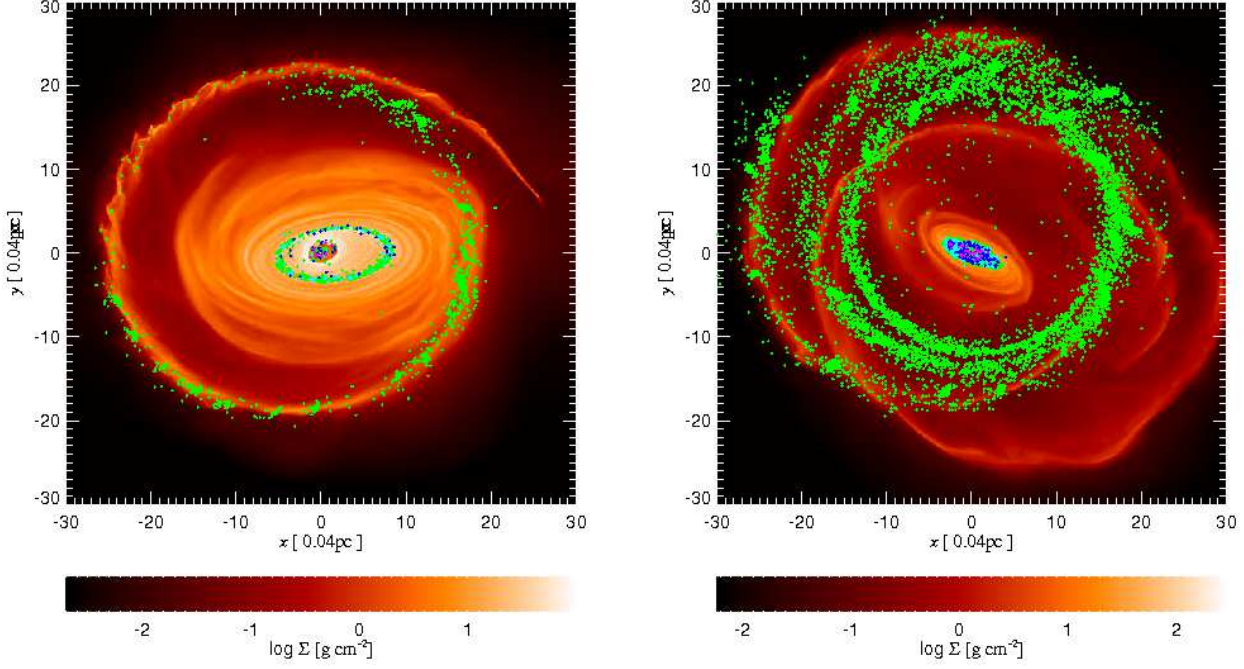


**Figure 5.** Projected gas densities and stellar positions for simulations S1 (left) and S2 (right) at  $t = 1955$ . Stars are shown by coloured symbols as following: green  $M_* = 0.1 - 1 M_\odot$ , cyan  $M_* = 1 - 10 M_\odot$ , blue  $M_* > 10 M_\odot$ , and magenta  $M_* > 150 M_\odot$ . Note the survival of the secondary filament in S2. The line of sight is along the  $z$ -direction.

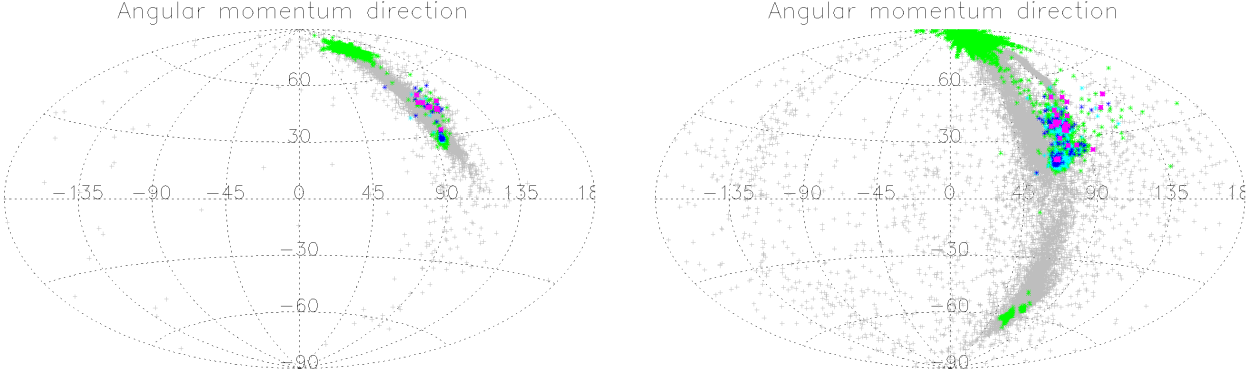


**Figure 6.** Angular momentum orientations for SPH particles (grey) and stars (colours as in Fig 5) in simulations S1 (left) and S2 (right) at  $t = 1955$ . Note that the inner stellar disc feature is rather small in angular extent i.e. thin and planar in the left panel, but is geometrically thick and significantly warped in the right.

through shocks and gravity. For the same reason, the filaments are much better defined in S3 than they are in S1. Similar conclusions can be drawn from comparison of runs S2 and S4.

#### 4.4.2 Star formation

Star formation occurs earlier in S3 than it does in S1. In particular, the first stars appear at  $t = 150$  in S3 and only at  $t \approx 1000$  in S1. This is expected since faster cooling facilitates faster gravitational collapse (e.g.,

Gammie, 2001; Rice et al., 2005). The S2 to S4 comparison is less extreme but still significant, with stars forming in S2 by  $t = 400$  and in S4 by  $t = 100$ . In both  $\beta = 0.3$  runs the initial sites of star formation were the orbiting gas filaments, with the disc stellar populations forming slightly later, at  $t = 350$  (S3) and  $t = 180$  (S4).

The clearly defined concentric ring structures of the S1 and S2 discs were also seen in S3 and S4, although they did not provide the sites of star formation in the latter cases, as fragmentation into sink particles occurred some time before the rings began forming. In terms of the stellar mass spectra

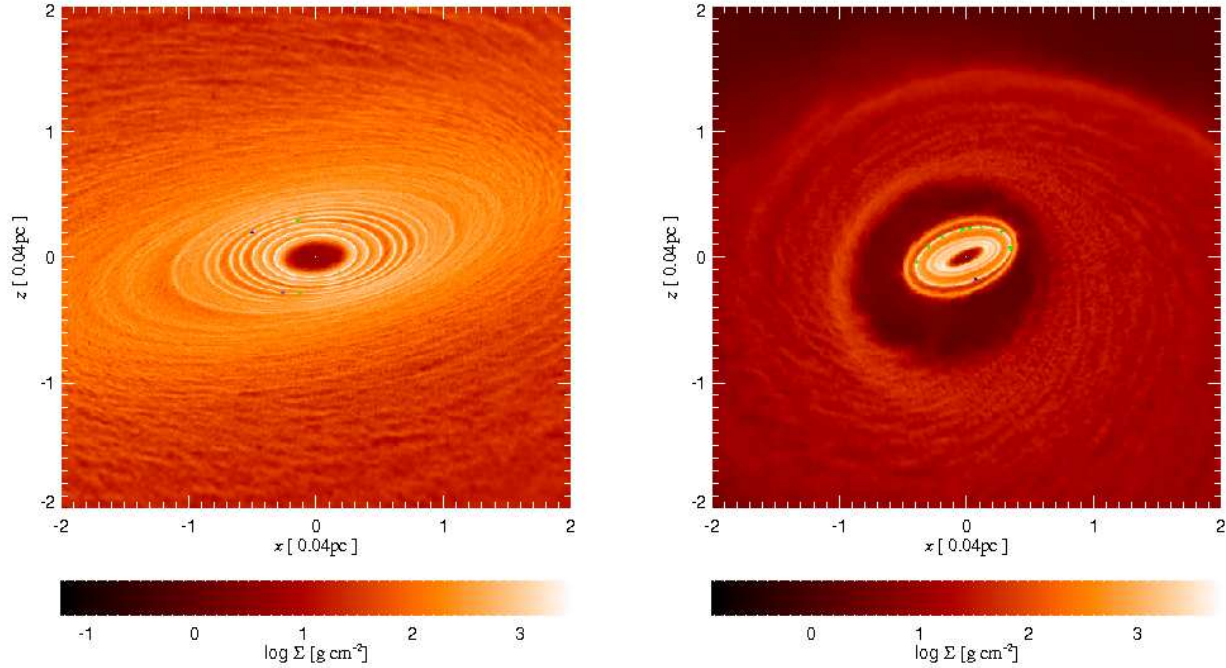


**Figure 7.** Projected gas density for the inner two arcseconds, showing stars forming (colours as in Fig 5). **Left:** Simulation S1 at  $t = 1000$ ; **Right:** Simulation S2 at  $t = 400$ . The times correspond to when first stars appear in these runs.

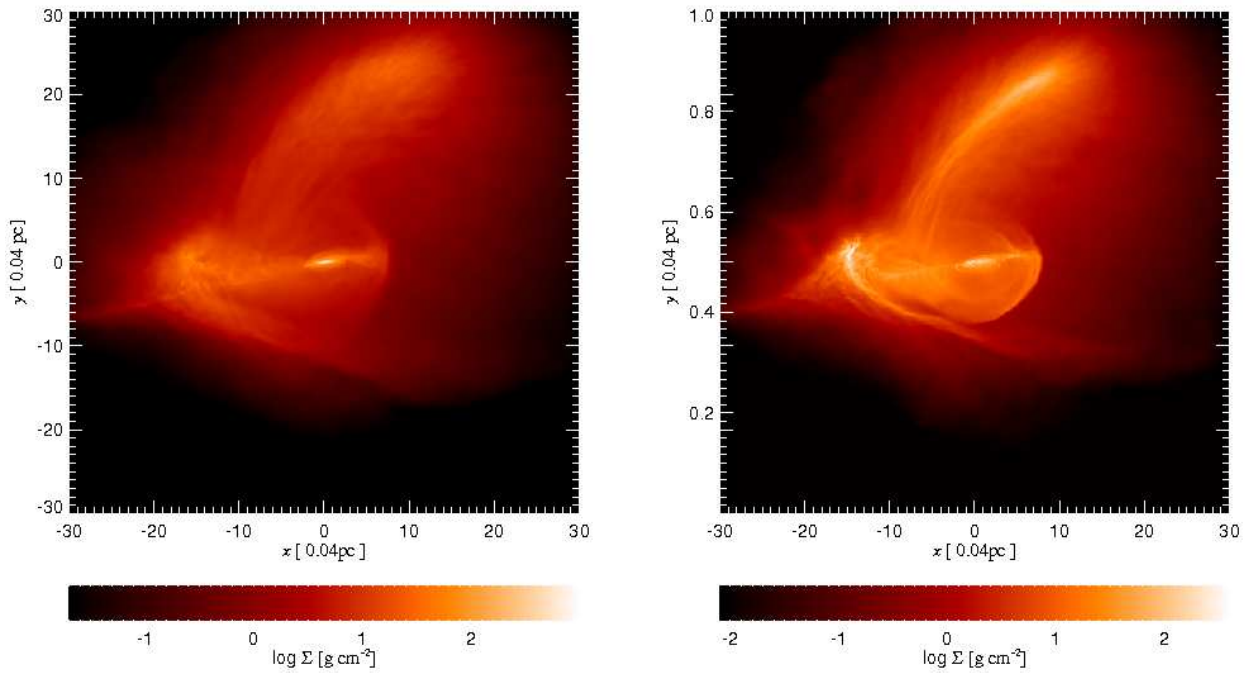


**Figure 9.** Comparison of projected gas density for simulation S1 (left panel,  $\beta = 1$ ) and S3 (right panel,  $\beta = 0.3$ ) at  $t = 150$ . Note that filamentary structures are denser and better defined in S3 than they are in S1.

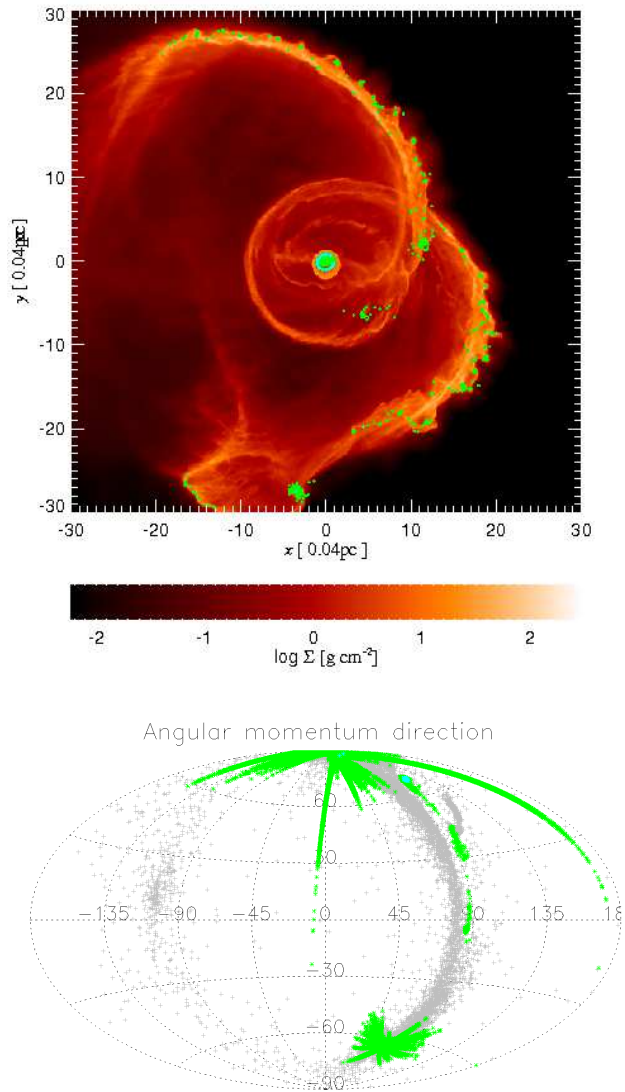


**Figure 10.** Projected gas density for simulation S4 (top) angular momentum of individual gas particles and stars (bottom) at time  $t = 360$ . In the angular momentum plot, gas is in grey whilst stars are colour-coded by mass, as they are in the gas density plot, as per 5. The extended stellar structures in angular momentum space, such as the linear features seen, correspond here to extremely compact “star clusters”. In the case of the most extended linear feature in the right-hand plot, velocity dispersion inside the cluster is comparable to its orbital velocity.

all the stars formed in S3 and S4 are low mass ( $\sim 0.1 - 1 M_{\odot}$ ), both in the filament populations and in the disc. Again, this is a natural consequence of a short cooling time (Nayakshin, 2006; Shlosman & Begelman, 1989).

#### 4.4.3 Clustered star formation

The top panel of Figure 10 shows the surface density of S4 some time after stars have begun to form. The bottom panel shows the orientation of the angular momentum of gas and star particles for the same snapshot. In contrast

to the equivalent plots for S1 and S2, one notices extended linear structures, “filaments” or “arms” in Figure 10. These structures, extended in angular momentum space, are in fact produced by the most compact features in coordinate space – the star clusters. These clusters are seen visually in the top panel of Figure 10. The velocity dispersion of the stars in these very dense clusters is high; some are comparable to the orbital velocities of the clusters themselves. For example, in the bottom panel of Figure 10, the two longest continuous “filaments”, separated by  $180^\circ$  in  $\phi$ , are produced by the densest and most massive cluster located at  $z \approx 0$ ,  $x = 4$ ,  $y \approx -28$  in the top panel. Due to its location close to the  $y$ -axis, the  $y$ -component of the angular momentum of any star that belongs to the cluster,  $l_y = -xv_z + zv_x \approx 0$ . Therefore the cluster’s stars form an incomplete plane  $l_y \approx 0$  in the angular momentum space, producing the two (actually one) very long “filaments” in the bottom panel of Figure 10. This cluster is a remnant of cloud 1, and its mass is  $\sim 3000$  solar masses.

In fact most of the stars in simulations S3 and S4 belong to a cluster. This clustered mode of star formation in the fast-cooling runs is due to the gas collapsing promptly and thus forming very massive dense gas halos. We suspect that these results would have been different had we been able to treat radiative feedback from star formation in our simulations. We note that in such a dense environment, any feedback from star formation activity, such as radiation or outflows, would not have been able to escape easily and would therefore have heated the surrounding gas, suppressing further fragmentation and increasing the Jeans mass (Nayakshin, 2006; Krumholz & Bonnell, 2007). Rather than the multiple low-mass stars in a cluster we would perhaps have seen fewer but higher mass stars. The mass spectrum of stars would probably also change if the colliding clouds had net rotation (spin) or a turbulent structure before the collision, providing some stability against collapse. All these effects are however minor as far as orbital motion of the stars is concerned, which is the focus of our paper.

#### 4.4.4 Inner fluctuating disc

Simulation S4 is the fast-cooling equivalent of S2. As such, the inner gaseous disc in S4 is subject to a similar intermittent infall of gas from larger radii. The newly arriving gas tweaks the disc orientation significantly, causing it to undergo midplane rotation (refer back to §4.3.1). The difference here however is that disc is fragmenting into stars whilst its orientation is changing. Interestingly, these stars do not follow the evolving disc orientation but rather remain in their original configuration. This is clearly seen in Figure 11, where the stellar disc remembers the “old” orientation of the gaseous disc in which the stars were born, whereas the gaseous disc evolves to quite a different orientation. The possibility of this effect taking place was suggested by Nayakshin & Cuadra (2005). These authors found that stars will not follow disc midplane changes if these occur faster than the “critical rotation time”, which is estimated to be about 500 code units for the disc in Figure 11. Our simulations are thus consistent with these predictions as the disc orientation changed on a timescale of just 80 code units.

As a result of a several star forming events in gaseous discs of different orientations, the inner stellar disc in S4 is



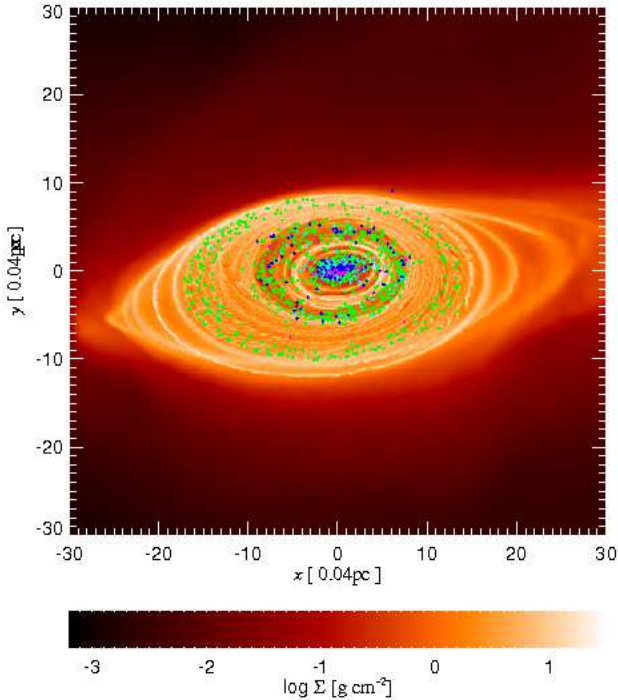


**Figure 12.** Projected gas density for S5 at  $t = 2696$ , showing stars as well (colours as in Fig 5). Note that the stellar populations all possess similar values for eccentricities.

very much different from that found in S2, and even more so when compared to S1. In the latter cases, when cooling is more gradual (i.e.  $\beta = 1$ ), stars only form in the inner gaseous disc once it has settled into a relatively stable orientation. Hence the resulting distribution of stars is correspondingly thin (although in S2 it is significantly thicker than S1, cf. Figure 6). Such a distribution is broadly consistent with the observed orbits of young massive stars in the clockwise disc in the GC (Paumard et al., 2006). Due to gaseous disc midplane changes coupled with quicker fragmentation, then, the stellar disc in S4 is much thicker, with  $H/R \sim 1$ . This particular simulation thus fails to account for the most prominent feature of the observational data; namely, a thin inner stellar disc.

#### 4.5 SIMULATIONS S5 & S6

Simulation S5 is somewhat distinct from all the rest due to its small impact parameter,  $b$ , between the gas clouds (see Table 1). As a result of this fact and the relatively large value of  $\beta$ , a higher degree of mixing is achieved. Figure 12 shows a snapshot from this simulation, showing both gas and stars. Compared with all the other runs, the accretion disc extends out to as much as  $R \sim 20$  and represents a very coherent disc with little warping. Outer gas filaments do not form due to an almost complete mixing of the original gas clouds.

This simulation is an excellent example of how just a small change in initial conditions can yield drastically different results. Comparing the parameters for S5 with those for S2 (refer to Table 1), we see that there are only rela-

tively minor differences (the largest one being the different in impact parameter). However, towards later times the behaviour of the gas diverges considerably, with S5 ending up with a single, extended disc and similarly-oriented stellar populations and S2 possessing a small, highly warped stellar disc together with outer stellar populations inclined at a large angle from each other.

Simulation S6 is again different in that it possesses the largest collision velocity of all the simulations, whilst retaining a cooling parameter of  $\beta = 1$ . One therefore expects the resulting thermal expansion of the clouds to significantly modify the velocities of the particles and encourage mixing. However, since the impact parameter is relatively large, this simulation actually has more in common with S2 than with S5, particularly in the inner parts where the gas forms into a double disc structure (refer back to §4.3.1). The gas dynamics are therefore largely equivalent to S2, and as such we will not discuss this simulation in detail.

#### 4.6 Star formation in rings

One particular interesting feature of our simulations is that the disc surface density exhibits slightly eccentric “rings” in the inner  $0.5 - 1''$ . Star formation occurs preferentially in these rings (see Figure 7) in the slower cooling runs. The inner discs in runs S1-S6 are eccentric, warped, with a radial gradient in both of these properties, and evolving under the influence of a continuous but variable infall of material from larger radii, in a fixed (BH + stellar cusp) potential. It is difficult to disentangle these various effects from one another to understand the origin of the rings in detail, but we believe that they are partly a consequence of a very fast cooling time (since  $t_{cool} \propto \beta r^{3/2}$ ) coupled with most likely a number of the above properties of the gas in the inner parts. We base this conclusion on our unsuccessful attempts to reproduce the rings in cleaner purpose-designed simulations. In particular we ran simulations with eccentric and circular, flat or warped discs, but found no ring structures. Similarly, Nayakshin et al. (2007) did not encounter such structures in their simulations of circular or eccentric self-gravitating discs. We plan to continue to investigate the cause of the rings, and in particular to determine whether they are a numerical or physical artifact. It should be noted at this point that the effect of the rings on our model and overall conclusions is (fortunately) negligible, as they only affect star formation within the inner  $\sim 0.5''$ , a region in which fragmentation would be suppressed through accretion luminosity (Nayakshin, 2006), if we were to include this in our model.

### 5 RADIAL DISTRIBUTION OF STARS

Interestingly, the most robust result from all of the 6 runs completed is the fact that distribution of stellar mass in an annulus,  $dM_* = \Sigma_*(R)2\pi R dR$ , versus radius roughly follows the law

$$\Sigma_*(R) \propto \frac{1}{R^2}. \quad (10)$$

We show these distributions for runs S1, S2, S3 and S5 (all the simulations that have progressed far enough to trans-

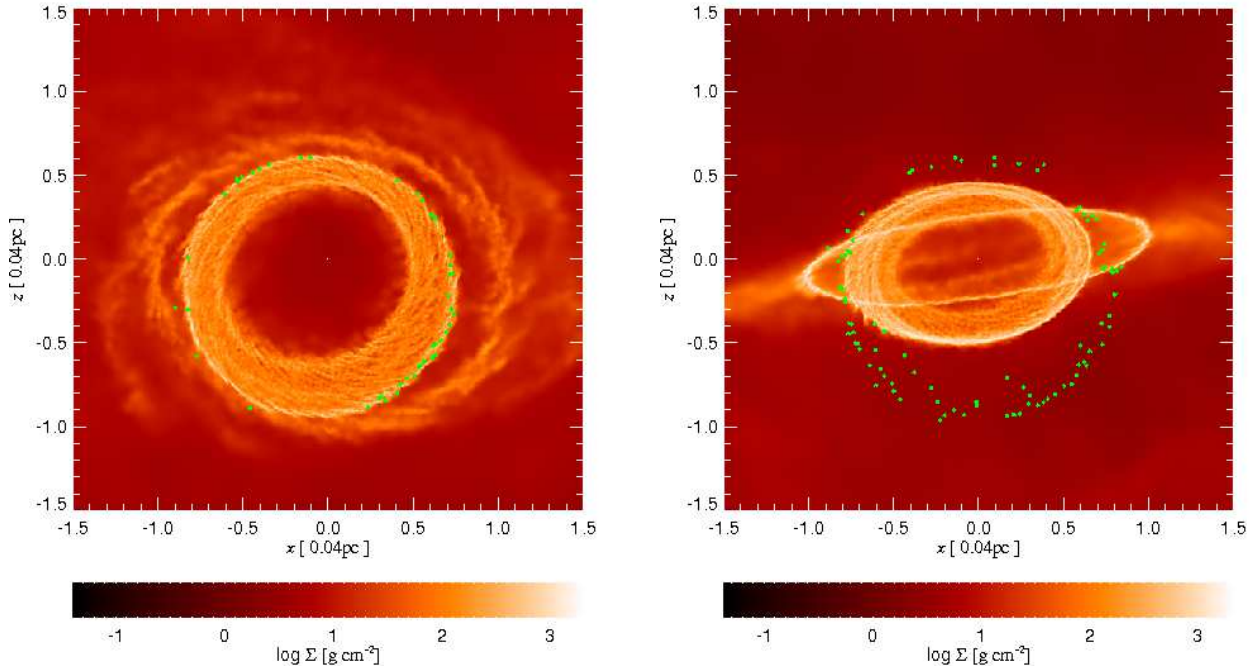


**Figure 11.** The inner 1.5 arcseconds of the simulation S4 at  $t = 180$  (left panel) and  $t = 260$  (right panel). Note that stars born in the gaseous disc at time earlier than  $t = 180$  kept their orbital orientation whereas the gaseous disc has evolved due to deposition of new matter from larger radii.

form a significant fraction of the gas into stars). To facilitate comparison with observational data, we use *projected* radius  $p$  instead of the proper 3D radius  $r$ , which is not directly known in observations of young stars in the GC (e.g., Genzel et al., 2003). As the viewing angle of the stellar system modelled here is arbitrary, we chose to plot the distributions along the three axes of the simulations, so that  $p = \sqrt{x^2 + y^2}$  for the black symbols,  $p = \sqrt{y^2 + z^2}$  for the red symbols, and  $p = \sqrt{x^2 + z^2}$  for the blue symbols. The lines in the Figure show  $R^{-2}$  (dotted) and  $R^{-3/5}$  (dashed) power laws. The latter corresponds to that predicted by *non self-gravitating* standard accretion disc theory.

This result is remarkable given very large differences in the 3D arrangements of the stellar structures in our simulations. The  $1/R^2$  law is in a good agreement with the observed distribution of “disc” stars (Paumard et al., 2006). Cancellations of angular momenta in shocks appears to be very efficient in driving gas to smaller radii. It would be interesting to explore a larger parameter space to quantify the robustness of these results.

## 6 SGR A\* FEEDING DURING AND AFTER THE CLOUD COLLISION

Figure 14 shows the mass accretion rate for the central black hole for simulations S1-S4. Formally, the Figure indicates that our simulations provide a sustained super-Eddington accretion rate (the Eddington accretion rate for Sgr A\* being  $\sim 0.03 M_\odot \text{ yr}^{-1}$ ), in some cases for between  $10^4$  to  $10^5$  yrs. However it must be remembered that we do not resolve gas dynamics inside the accretion radius. We expect that

material will form a disc there, and accretion will proceed viscously. The viscous time scale,  $t_{\text{visc}}$ , depends on the temperature in the disc midplane and the viscosity parameter,  $\alpha$  (Shakura & Sunyaev, 1973). The midplane temperature in the inner arcsecond is around  $10^3 \text{ K}$  in both the standard (non self-gravitating, e.g., Nayakshin & Cuadra, 2005) and the self-gravitating regimes (Nayakshin, 2006), yielding  $H/R \sim 0.01$ . Hence the viscous time is

$$t_{\text{visc}} = 6 \times 10^6 \text{ years } \alpha_{0.1}^{-1} \left[ \frac{R}{100H} \right]^2 r^{3/2}, \quad (11)$$

where  $\alpha_{0.1} = \alpha/0.1$  and  $r$  is in our code units (arcseconds). With these fiducial numbers, the viscous timescale coincides with the age of the young massive stars in the GC (e.g., Krabbe et al., 1995; Paumard et al., 2006). As  $\alpha$  is highly uncertain, we shall then consider the two opposite cases. If  $\alpha = 0.1$ ,  $t_{\text{visc}} \lesssim$  a few million years ( $\approx 10^6$  years at  $0.2''$ ), and we expect that gas would have mainly accreted onto Sgr A\* by now. This accretion rate would be a significant fraction of the Eddington accretion rate. Standard disc accretion would then generate as much as  $2 \times 10^{56} \text{ erg } M_{\text{acc},3}$  of radiative energy, where  $M_{\text{acc},3}$  is the gas mass accreted by Sgr A\* in units of  $10^3 M_\odot$ . A similar amount of energy could have been released as energetic outflows. There is currently no evidence for such a bright and relatively recent period of accretion activity for Sgr A\*.

In the opposite limit, i.e. if  $\alpha \ll 0.1$ , and  $t_{\text{visc}} \gtrsim$  a few million years, a gaseous disc should still be present as self-consistent modelling predicts that stars should not be forming inside  $r \lesssim 0.3'' - 1''$  (Nayakshin, 2006; Levin, 2006). There are however very strong observational con-

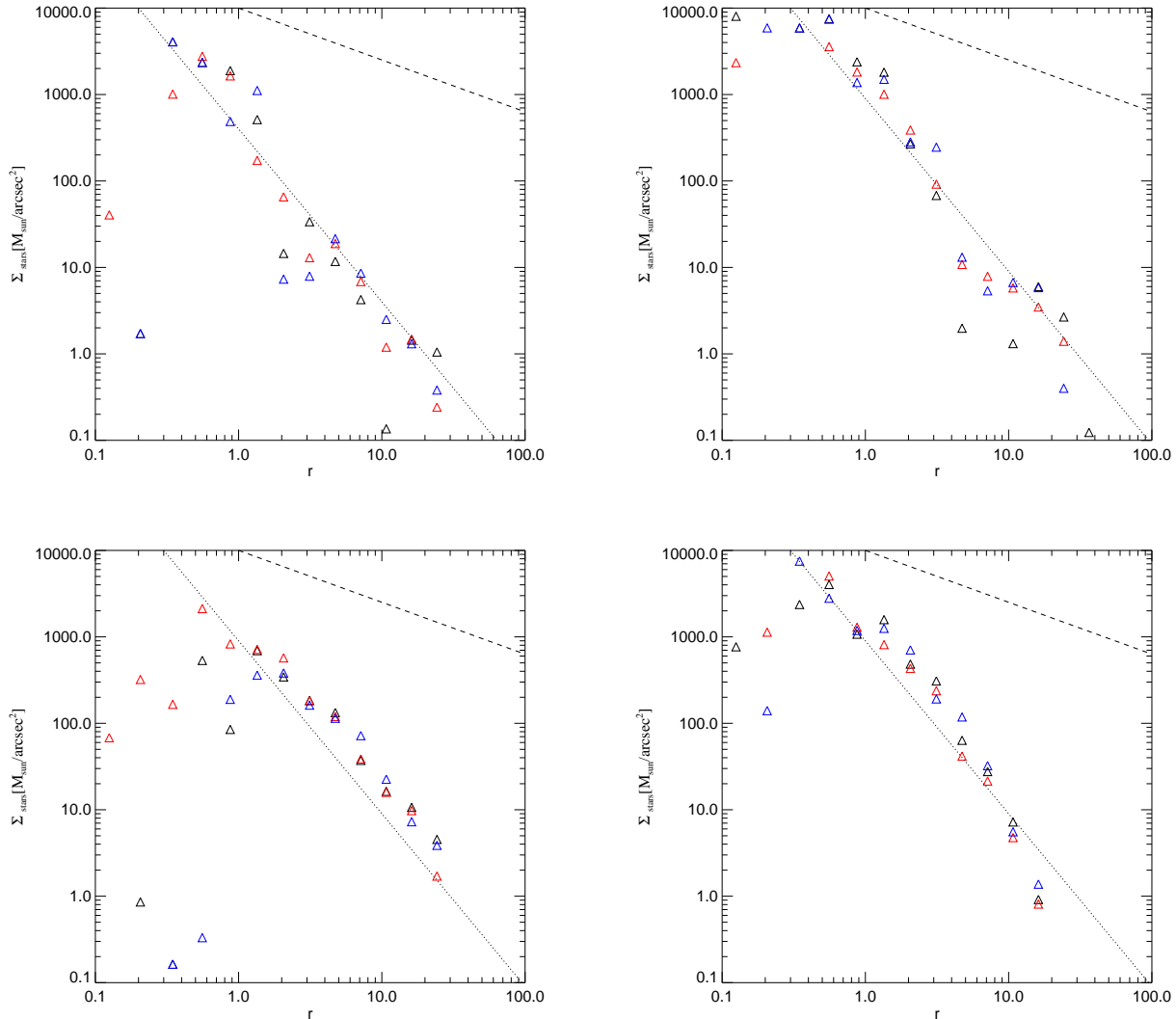


**Figure 13.** Stellar surface density,  $\Sigma_*$ , versus projected radius, for runs S1 (top left, at  $t = 1955$ ), S2 (top right, at  $t = 2243$ ), S3 (bottom left, at  $t = 1396$ ) and S5 (bottom right, at  $t = 2696$ ). Different colours show the three different orientations, along  $z$ ,  $x$  and  $y$  axes (black, red, and blue respectively). Power laws are overlaid for  $R^{-2}$  (dotted) and  $R^{-3/5}$  (dashed). All four plots correspond to the maximum time to which each simulation has been run.

straints on the absence of such a massive gaseous disc in the inner arcsecond of our Galaxy (e.g., Falcke & Melia, 1997; Narayan, 2002; Cuadra et al., 2003).

Therefore, our simulations seem to over-predict the amount of gaseous material deposited in the inner  $\sim 0.3''$ . We take this as an indication that a better model would perhaps involve a gaseous cloud of a larger geometric size, thus shifting all spatial scales outwards (see further discussion of this in §7.2).

## 7 DISCUSSION

### 7.1 Summary of main results

In terms of the final distribution of gas and resulting stellar populations, our results can be divided into two main categories.

(i) For those runs with a relatively small impact parameter, namely S1, S3 and S5, the initially small-scale disc around the black hole grows by steady accumulation of gas to extend out to  $r \sim 15''$ . As a result, more than one stellar population is seen in the disc. In addition to the ubiquitous stars in the inner few arcseconds, a “mid-range” population is seen, at  $r \sim 5 - 8''$ . Populations in the filaments vary: in S1, only the primary filament forms a stellar population, as the secondary has accreted onto the disc by the time stars begin to form; in S3, although the gas dynamics are the same, the secondary filament forms stars before it can accrete, resulting in two filamentary populations; and in S5, due to the small impact parameter a single large disc is created, resulting in three disc stellar populations all at a similar orientation.

(ii) For the runs with a larger impact parameter, namely S2, S4 and S6, the small-scale disc grows very little over



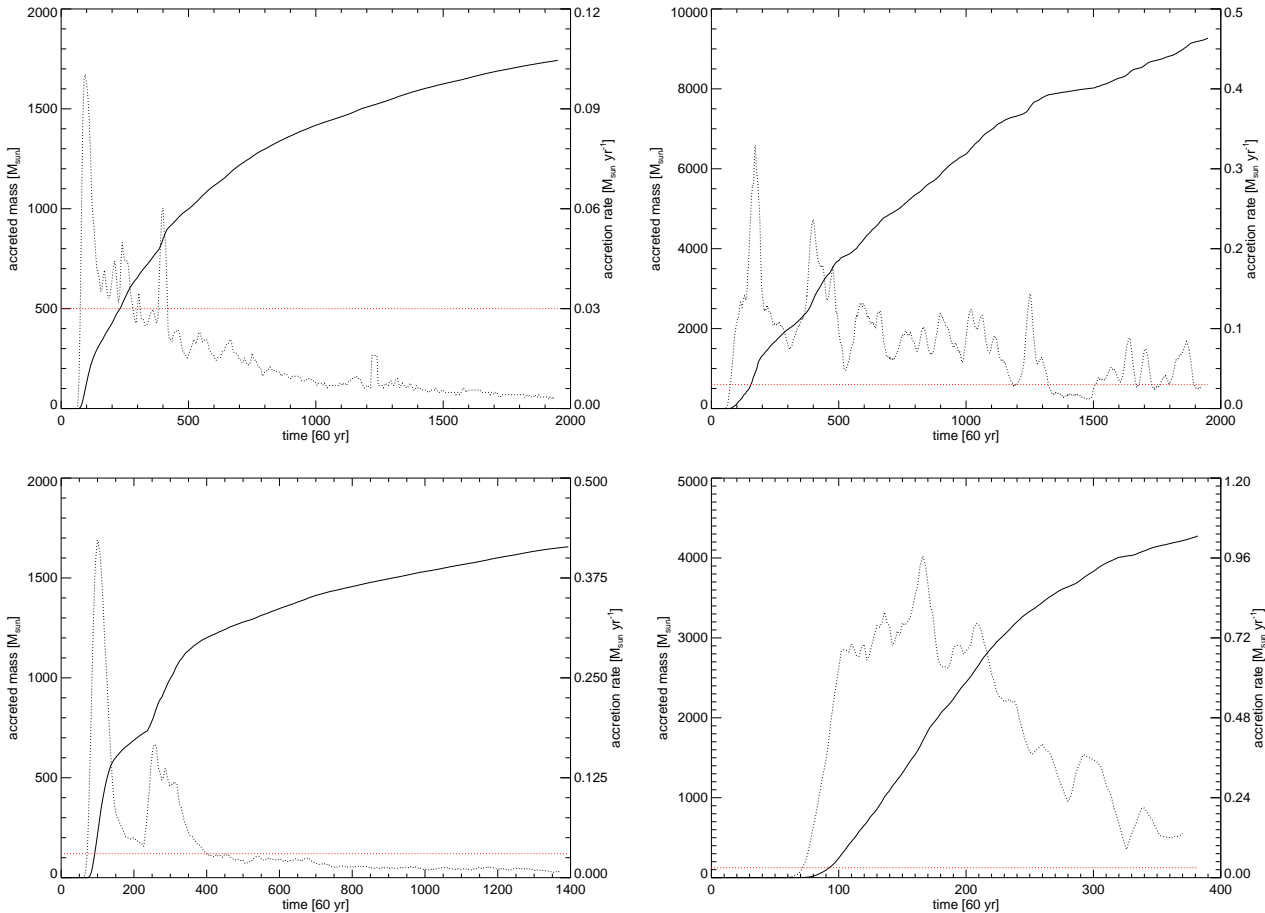


**Figure 14.** The time evolution of the accreted mass onto the central black hole (solid line) and the corresponding accretion rate (dotted line) compared to the Eddington limit for Sgr A\* (dotted red line), for simulations S1 (top left), S2 (top right), S3 (bottom left), and S4 (bottom right)

the course of the simulation, staying within a radius of a few arcseconds. The feeding of the disc is far from steady, generating enhanced midplane rotation, which, coupled with star formation (particularly in the case of faster cooling, e.g., S4) results in geometrically thick stellar populations. Both the primary and secondary filaments survive, and each form stellar populations inclined at a large angle to each other.

The other results of our simulations, presented roughly in the order of their commonality to the 6 simulations, are the following. Firstly, the formation of a gaseous nearly circular disc in the inner region of the computational domain is common to all runs, as is the ensuing formation of stars on similar circular orbits. This is natural as the dynamical time in the innermost disc is only  $\sim 60r^{3/2}$  years. On the scale of the inner disc,  $r \sim 1$ , the disc makes tens to hundreds of revolutions during the simulation, allowing for a near circularisation of the gaseous orbits. Conversely, the outer gaseous stream becomes self-gravitating much faster than it could circularise (or even become an eccentric disc), and hence orbits of stars in that region are more eccentric. This division on inner circular and eccentric outer orbits is in broad agreement with the properties of the observed orbits (Paumard et al., 2006). One discrepancy however is the eccentricity of the counter-clockwise feature of the ob-

servations compared to the outer stellar populations as seen in our model; the former is believed to possess a value of  $e \sim 0.6 - 0.8$  whilst the latter we find is only  $e \sim 0.2 - 0.4$ . We believe that simulations that use a strongly eccentric initial orbit for one of the clouds should be able to match the observations more closely.

Another robust result of our simulations is that all of the gaseous and ensuing stellar discs are significantly warped, by between  $30^\circ$  to  $60^\circ$  measured from the inner to the outer radii. Interestingly, most recent analysis of the observations reveals strong warps in the clockwise disc system (Bartko et al 08, private communication).

We also found that the radial distribution of stellar mass closely follows the observed  $\Sigma_* \propto 1/R^2$  profile of the disc stellar populations (Paumard et al., 2006). This was observed for all the simulations, although we expect these results would change if the colliding clouds moved in similar directions, significantly reducing the angular momentum cancellation in the shock and the thermal “kick” velocity due to the shock. Of course, this latter setup would prevent the formation of stellar populations at a large angle of inclination with respect to each other (one of the most prominent features of the observational data), so it is reasonable that we have not tested this possibility in our model.

For the same initial configurations, simulations with a comparatively long cooling time parameter,  $\beta = 1$ , lead to kinematically less dispersed stellar populations than those with faster cooling (i.e.,  $\beta = 0.3$ ). As a result, the longer the cooling time, the more closely the resulting stellar system can be fit by planar systems in velocity space. The innermost stellar disc is then reminiscent of the observed clockwise *thin* stellar system (Paumard et al., 2006) in terms of stellar orbits. Rapid cooling produces clumpier gas flows that lead to significant gaseous disc orientation changes during the simulations. Rapidly cooling gas flows naturally form less coherent discs; such geometrically thick systems are incompatible with the observations.

Interestingly, with the chosen initial conditions, faster cooling promotes survival of the gaseous streams corresponding to the orbits of the original clouds. These streams fragment and form stars mainly in a clustered mode, although this might be expected to depend on the details of the radiation feedback from young stars, which is not modelled in this set of simulations.

Our slower cooling runs produce inner and outer stellar systems that are inclined to each other by only about  $40^\circ$ , which is much smaller than the observed angle of  $\sim 110^\circ$  between the discs (Paumard et al., 2006). This is a natural consequence of angular momentum conservation in a “viscous”, well-mixed gas flow – the disc orientation in our model will always lie in-between the positions of the initial clouds in angular momentum space.

## 7.2 Origin of the observed stars: one or two clouds?

None of our runs reproduce the observed properties of stars and their orbits in detail. This is not surprising as the parameter space for initial conditions is quite large, and we have explored only a tiny fraction of it here. We feel, however, that the agreement with the observations is encouraging and that the model is promising. To quantify this discussion here, we must note that the observational picture itself is still not entirely clear. Whereas Genzel et al. (2003) and Paumard et al. (2006) classify the orbital stellar distribution as two discs, the statistical significance of the second disc is disputed by Lu et al. (2006) Lu et al. (2008). Although we tend to agree with the first opinion, we shall consider both of these possibilities without bias here.

Let us first discuss the origin of the clockwise stellar disc in the inner parsec of the GC. The existence of this disc is not in question since the work of Levin & Beloborodov (2003) and Genzel et al. (2003). Concentrating on this feature *only*, a viable model can be simplified to a self-collision of a large molecular cloud rather than collision of two clouds. Recently, Wardle & Yusef-Zadeh (2008), argued that a viable progenitor for the stellar discs is a large-scale molecular cloud, such as the  $50 \text{ km s}^{-1}$  GMC actually observed near the GC. In this model, the cloud infalls almost radially onto Sgr A\*, temporarily engulfing the SMBH. While most of the cloud nearly passes by, gas within one parsec or so gets captured by the SMBH and settles into a bound disc of gas. This model may be also useful in explaining not only the observed stellar disc within the inner parsec but also the CND further out at  $\sim 10 \text{ pc}$ .

Even more recently, Bonnell & Rice (2008) have per-

formed numerical simulations of a scenario similar to that suggested by Wardle & Yusef-Zadeh (2008). In particular, an infalling turbulent molecular cloud was set on a sub-parsec impact parameter with respect to the SMBH. While their numerical method did not include radiative transfer directly (it is of course also not included here), they did use an effective equation of state that to some degree mimics the radiative effects. It was found that the cloud becomes tidally disrupted and forms an eccentric disc around the SMBH. This disc later fragmented into stars with a top-heavy IMF resulting from inefficient cooling. Therefore, the one cloud scenario appears to be attractive both qualitatively and quantitatively as an explanation for the origin of the clockwise stellar disc.

Now, considering the rest of the young massive stars that do *not* belong to the clockwise disc kinematically, we note that these account for no less than 50% of the overall stellar population. Whether the majority of these stars form the second disc or not, their velocity vectors differ from the clockwise disc by up to a few hundred km/sec (which is the order of circular velocity at these distances). The velocity dispersion even in a very compact Giant Molecular Cloud, with mass of say  $3 \times 10^4 M_\odot$  and size of 1 pc, is only  $\sim 10 \text{ km/sec}$ . Thus the only way to create the observed kinematically distinct population of stars would be to postulate the existence of two or more streams (filaments) inside the cloud that pass on opposite sides of Sgr A\* and do *not* get completely mixed before forming stars. Given our numerical experiments in this paper, this does not seem implausible if the cooling time is short  $\beta \lesssim 1$ . What is interesting in this scenario is that the massive stars of the counter-clockwise population would then have to form very quickly, i.e., on a dynamical timescale, or else gaseous orbits would be mixed. The rotation period scales approximately as  $T_{\text{rot}} = 3000(R/5'')^{3/2}$  years, so this is quite fast indeed.

In contrast, in the case of the collision of two clouds as considered here, it is almost too easy to obtain the inner circular disc and a very diverse stellar population farther out. We therefore favor a model where a GMC did collide with a pre-existing cloud or structure, such as a massive larger-scale disc, e.g., similar to the observed CND.

## 7.3 Size of the cloud(s)

The observed well defined, flat, geometrically thin and almost circular clockwise stellar system (Paumard et al., 2006) is best created via a gentle accumulation of gas. Several independent major gas deposition events lead to a warped disc, and/or mixed systems consisting of several stellar rings or discs co-existing at the same radius. To avoid this happening, the inner disc must be created on time scale longer than the critical rotation time, which is estimated at  $t_{\text{cr}} \sim \text{few} \times 10^4$  years.

While these results are based on analytical arguments (Nayakshin & Cuadra, 2005) and our simplified one-parameter  $\beta$ -cooling model, we note that the results of Bonnell & Rice (2008) corroborate this as their inner stellar disc appears to be too eccentric to match the data of Paumard et al. (2006).

Deposition of gas in the inner disc takes place on the longest of two timescales: the cooling time  $t_{\text{cool}}$  and the collision time,  $t_{\text{coll}} \sim R_{\text{cl}}/v_{\text{cl}}$ , where  $R_{\text{cl}}$  and  $v_{\text{cl}}$  are the cloud’s

size and velocity magnitude. In the appendix we estimate the realistic cloud cooling time *during the collision*, and show that it is always much shorter than the dynamical time unless magnetic fields are very important.

We are thus left with the only option to require the collision itself be more prolonged than  $t_{\text{cr}}$ . Estimating the velocity of the cloud at  $v_{\text{cl}} \sim 150$  km/sec, which is of order of circular velocities in the inner Galaxy outside the inner parsec, we find  $t_{\text{coll}} = R_{\text{cl}}/v_{\text{cl}} \sim 10^4 \text{ years } R_{\text{cl,pc}}$ , where  $R_{\text{cl,pc}}$  is the size of the cloud in parsecs. We hence require the cloud to be larger than a few parsecs to satisfy  $t_{\text{coll}} \gtrsim t_{\text{cr}}$ . Note that this size is not necessarily the original size of the cloud if the cloud gets tidally disrupted before it makes the impact. In the latter case we can take  $R_{\text{cl}}$  to be the radial distance to the centre of the Galaxy at which the tidal disruption took place. Finally, the location of the collision should not be too far from the central parsec, or else too much angular momentum would have to be lost to deposit a significant amount of gas at  $\sim 0.1$  pc.

Another argument going in the same direction comes from a comparison of the radial distribution of gas and stars in our simulations with the observed stellar distribution (Paumard et al., 2006). The former is too compact, i.e., all of our simulations deposited *too much* mass within the inner arcsecond. In addition, if that was indeed the case 6 million years ago, then Sgr A\* would have received a significant amount of fuel, enough to become at least a bright AGN. Given the long viscous times in the inner arcsecond, Sgr A\* could actually continue to accrete this fuel now. However, it is well known that there is no geometrically thin and optically thick disc inside the inner arcsecond of Sgr A\* (Falcke & Melia, 1997; Narayan, 2002; Cuadra et al., 2003). Eliminating the gaseous disc by star formation is not an option as there are not enough massive young stars observed there.

Taking all these constraints together, we believe that the most realistic scenario would be a GMC of the order of a few parsecs in size striking the CND at the distance of a few parsecs from Sgr A\*. This scenario could perhaps explain the origin of the inner edge of the CND at  $R \approx 2$  pc if the refilling time scale is longer than the age of the young stars. Alternatively such a cloud could self-collide if the impact parameter with respect to Sgr A\* is small enough, but the cloud needs to be very structured, e.g., essentially consist of several smaller clouds or filaments.

## 8 CONCLUSIONS

In this paper we presented several simulations of cloud-cloud collisions aimed at reproducing gas flows that could have formed (a) gaseous disc(s) in the central parsec of our Galaxy, as well as the resulting star formation. We found the gas cooling time and the impact parameter of the collision to influence the outcome significantly. Nevertheless, there are several robust results: (a) the inner circular and outer eccentric orbital structure of the stars formed there; (b) a sharply peaked mass distribution of stars  $\Sigma_*(R) \sim 1/R^2$ ; (c) that the gaseous and stellar discs are warped. These results are in good accordance with the observations. The breakdown of the stellar system into one or more components is sensitive to the initial conditions and also the cooling parameter.

It appears that a GMC with a size of one to a few parsecs, self-colliding on a nearly radial orbit, or striking the CND at the distance of a few parsec from Sgr A\* could explain the known observational data satisfactorily. Future observations and modelling might put interesting upper limits on the timescale over which the massive stars formed in the GC, and detail the structure and orbit of such a GMC.

## 9 ACKNOWLEDGMENTS

We acknowledge useful comments on the draft by Peter Cossins, Giuseppe Lodato and Yuri Levin.

## REFERENCES

- Alexander R. D., Armitage P. J., Cuadra J., 2008, ArXiv e-prints, 807
- Baganoff F. K., Maeda Y., Morris M., et al., 2003, ApJ, 591, 891
- Bate M. R., Bonnell I. A., Price N. M., 1995, MNRAS, 277, 362
- Bonnell I. A., Rice W. K. M., 2008, Science, 321, 1060
- Collin S., Zahn J., 1999, A&A, 344, 433
- Cuadra J., Nayakshin S., Sunyaev R., 2003, A&A, 411, 405
- Deegan P., Nayakshin S., 2007, MNRAS, 377, 897
- Demircan O., Kahraman G., 1991, Astrophysics and Space Science, 181, 313
- Eisenhauer F., Genzel R., Alexander T., et al., 2005, ApJ, 628, 246
- Falcke H., Melia F., 1997, ApJ, 479, 740
- Figer D. F., 2004, in ASP Conf. Ser. 322: The Formation and Evolution of Massive Young Star Clusters, 49–+
- Frank J., King A., Raine D. J., 2002, Accretion Power in Astrophysics: Third Edition, Accretion Power in Astrophysics, by Juhan Frank and Andrew King and Derek Raine, pp. 398. ISBN 0521620538. Cambridge, UK: Cambridge University Press, February 2002.
- Freitag M., Amaro-Seoane P., Kalogera V., 2006, ApJ, 649, 91
- Gammie C. F., 2001, ApJ, 553, 174
- Genzel R., Schödel R., Ott T., et al., 2003, ApJ, 594, 812
- Gerhard O., 2001, ApJ, 546, L39
- Ghez A. M., Duchêne G., Matthews K., et al., 2003, ApJ, 586, L127
- Ghez A. M., Salim S., Hornstein S. D., et al., 2005, ApJ, 620, 744
- Goodman J., 2003, MNRAS, 339, 937
- Gorda S. Y., Svechnikov M. A., 1998, Astronomy Reports, 42, 793
- Gürkan M. A., Rasio F. A., 2005, ApJ, 628, 236
- Hansen B. M. S., Milosavljević M., 2003, ApJ, 593, L77
- Hasegawa T., Sato F., Whiteoak J. B., Miyawaki R., 1994, ApJL, 429, L77
- Hopman C., Alexander T., 2006, ApJL, 645, L133
- Kim S. S., Figer D. F., Morris M., 2004, ApJ, 607, L123
- Kolykhalov P. I., Sunyaev R. A., 1980, Soviet Astron. Lett., 6, 357
- Krabbe A., Genzel R., Eckart A., et al., 1995, ApJ, 447, L95
- Krumholz M. R., Bonnell I. A., 2007, ArXiv e-prints, 712
- Levin Y., 2006, ArXiv Astrophysics e-prints, astro-ph/0603583
- Levin Y., Beloborodov A. M., 2003, ApJ, 590, L33
- Levin Y., Wu A., Thommes E., 2005, ApJ, 635, 341
- Lu J., Ghez A., Hornstein S., et al., 2006, JPhCS, 54, 279
- Lu J. R., Ghez A. M., Hornstein S. D., Morris M. R., Becklin E. E., Matthews K., 2008, ArXiv e-prints, 808
- Miralda-Escudé J., Gould A., 2000, ApJ, 545, 847
- Miyoshi M., Moran J., Herrnstein J., et al., 1995, Nature, 373, 127
- Morris M., 1993, ApJ, 408, 496

- Narayan R., 2002, in *Lighthouses of the universe: the most luminous celestial objects and their use for cosmology*, ed. M. Gilfanov, R. Sunyaev & E. Churazov (Berlin: Springer), 405
- Nayakshin S., 2006, *MNRAS*, 372, 143
- Nayakshin S., Cuadra J., 2005, *A&A*, 437, 437
- Nayakshin S., Cuadra J., Springel V., 2007, *MNRAS*, 379, 21
- Nayakshin S., Dehnen W., Cuadra J., Genzel R., 2006, *MNRAS*, 366, 1410
- Nayakshin S., Sunyaev R., 2005, *MNRAS*, 364, L23
- Paczynski B., 1978, *Acta Astron.*, 28, 91
- Paumard T., Genzel R., Martins F., et al., 2006, *ApJ*, 643, 1011
- Paumard T., Maillard J.-P., Morris M., 2004, *A&A*, 426, 81
- Reid M. J., Readhead A. C. S., Vermeulen R. C., Treuhaft R. N., 1999, *ApJ*, 524, 816
- Rice W. K. M., Lodato G., Armitage P. J., 2005, *MNRAS*, 364, L56
- Schödel R., Ott T., Genzel R., et al., 2002, *Nature*, 419, 694
- Schödel R., Eckart A., Alexander T., et al., 2007, *A&A*, 469, 125
- Shakura N. I., Sunyaev R. A., 1973, *A&A*, 24, 337
- Shlosman I., Begelman M. C., 1989, *ApJ*, 341, 685
- Springel V., 2005, *MNRAS*, 364, 1105
- Stolte A., Ghez A. M., Morris M., Lu J. R., Brandner W., Matthews K., 2008, *ApJ*, 675, 1278
- Wardle M., Yusef-Zadeh F., 2008, *ApJL*

magnitude. The strongly increased magnetic pressure might present another form of energy and pressure support against gravitational collapse. If magnetic flux is then removed from the cloud by magnetic buoyancy instability, this happens on time scales longer than dynamical, effectively implying large values of  $\beta$ .

Summarising, a realistic value of  $\beta$  during the initial cloud-cloud collision would be very small if magnetic fields are not important, or large if strong field amplification occurs due to the shock.

## APPENDIX A: ON REALISTIC ESTIMATES OF THE COOLING TIME DURING THE CLOUD COLLISION

Here we try to estimate the realistic cooling time for the gas clouds in the initial collision event. Clouds moving at a few hundred km/sec would yield a maximum shock temperature of a few million K. Using the optically thin cooling function at these temperatures (dominated by Bremsstrahlung and metal line cooling) and initial cloud densities, one finds that the optically thin cooling time is 3 – 5 orders of magnitude shorter than dynamical time at  $R \sim 25''$ , the latter being  $t_{\text{dyn}} = 8 \times 10^3$  yrs. With our chosen parameters for the initial conditions, the clouds are Compton-thick, i.e.  $\Sigma \sim$  a few tens of  $\text{g cm}^{-2}$ . The shock would emit soft X-rays through Bremsstrahlung, which would have an absorption opacity much higher than that of the Thompson opacity i.e.  $\kappa_{\text{T}} = 0.4 \text{ cm}^2 \text{ g}^{-1}$ . These X-rays would therefore be completely absorbed within the colliding clouds. This would not lead to a significant increase in the cooling time, however, as the absorbed X-rays would be re-emitted as thermalised blackbody emission at the effective temperature of the radiation. The latter is estimated to be around  $10^3$  K. The clouds' optical depth to such radiation is of the order of a few tens, meaning that the clouds would still be able to cool effectively via blackbody emission. The cooling time for the cloud in its entirety would therefore remain short (using the Stefan-Boltzmann law for radiative emission,  $t_{\text{cool}}$  would again be  $\sim 3$  orders of magnitude shorter than  $t_{\text{dyn}}$ ).

However, as was pointed out to us by Yuri Levin, these considerations completely neglect magnetic fields that are most likely present in the pre-collision clouds. If the radiative cooling time is short, then the shock is essentially isothermal, and we can expect the gas to be compressed in the shock by a few orders of magnitude for our typical conditions. A frozen-in magnetic field would then be amplified by similar factors, and magnetic pressure by four to six orders of